PAPER • **OPEN ACCESS**

Optical and Thermophysical Characterization of Fe_3O_4 nanoparticle

To cite this article: F Horia *et al* 2020 *IOP Conf. Ser.: Mater. Sci. Eng.* **956** 012016

IOP Conf. Series: Materials Science and Engineering **956** (2020) 012016 doi:10.1088/1757-899X/956/1/012016

Optical and Thermophysical Characterization of Fe_3O_4 nanoparticle

Horia.F [1], Khaled Easawi [1], Reda Khalil[2], Said Abdallah [1], Mabrouk El-Mansy[2], and Sohair Negm[1]

[1] Department of Mathematical and Physical Engineering, Faculty of Engineering (Shoubra), Benha University, Cairo, Egypt

[2] Physics Department, Faculty of Science, Benha University

*horya.omer@feng.bu.edu.eg

Abstract

The size dependence of optical and, thermophysical properties of Fe_3O_4 nanoparticle (NPs) has been investigated. Three samples of Fe_3O_4 NPs with different sizes were prepared by the Co-precipitation method and labeled a, b and c. The UV- vis spectra shifted toward the lower energy with increasing the particles size. The energy bandgaps of the synthesized Fe_3O_4 NPs are 1.84 ev,1,73 ev, and 1,47 ev for a, b and c respectively. The sizes of the nanoparticles were estimated using the effective mass approximation (EMA) model, and are 10.7 nm, 20.56 nm, and 30.43 nm. These values are comparable to those found by transmission electron microscope (TEM) and X-ray diffraction (XRD). The Photoacoustic (PA) technique was used to research Fe_3O_4 NPs for thermal diffusivity (α), thermal effusivity (e), and thermal conductivity (k). The determined values of α, e, and k increase as the size of nanoparticles rises and decreases from the bulk by about 33%.

Keywords

Photoacoustic spectroscopy, Magnetite, The thermal conductivity, Thermal diffusivity

1. Introduction.

Metal oxides are commonly studied due to their unique electrical and chemical stability, thermal optical, magnetic and rheological, catalytic properties [1]. Ferrites have widespread applications in electronics [2], magneto-optics [3], magnetocaloric refrigeration [4], dynamic sealing, high-density data storage [5], oscillation damping, and catalysis [6–8]. From nanocrystalline ferrites, Fe_3O_4 is the ideal candidate for various biomedical applications because of its cell and biomolecular dimensions [9], low toxicity [10], biocompatibility [11], high saturation magnetization, and easy to control with low magnetic fields [12]. Fe_3o_4 Magnetic particles have physical and chemical properties which could be applied in different fields by transforming them into particles of nanometer scale. These nanoparticles may be used as drug delivery (DDS), magnetic resonance imaging (MRI), and cancer therapy products. The nature of nanoparticles' particle size, magnetic properties, and surface properties was very important for it to be applied to the field [13]. Thermal conductivity was a physical property of a material which shows the ease with substances which could achieve heat energy transmission with molecular motion thermal conductivity of material depending on the substance's chemical composition, the solid 's crystalline structure, the temperature and the pressure under which it was imposed [14]. Massive attention has therefore been paid to investigating its thermal properties to boost the efficiency of solar cell devices and pave the way for new applications as well. [15]. Since the mid-1970, the use of photoacoustic spectroscopy (PAS) to obtain absorption spectrums of solid and fluid substances has attracted considerable interest. The primary source of PA signal results from a periodic heat flow from the solid to the surrounding gas. These can be explained when the beam of light falls on to the sample, the heat produced by the light absorbed in the sample (created by means of non-radiative transition) will diffuse from the sample to the gas through the sample- gas interference. By modulating the light beam, the expansions of the gas layer near the sample create a sound wave transferred

from the gas to the microphone [16]. Therefore, the PA signal contains information about the optical absorption within the sample in addition to the way with which the heat is diffused through the sample. The Rosencwaig and Gersho (RG) theory of the PA effect [17] shows that the pressure variations depend on the optical and thermal parameters of the sample. This study aims to synthesize Magnetite Fe_3O_4 NPs of various sizes using the process of co-precipitation. The size-dependent UV-vis spectra have been investigated. The energy band gap of Fe_3O_4 NPs of different sizes was measured. The sizes of nanoparticles have been estimated using effective mass approximation (EMA) [18] and verified by XRD and TEM. Furthermore, thermal diffusivity (α), thermal effusivity (e), and thermal conductivity (k) of different sizes of Fe_3O_4 NPs have been measured using the non-destructive photoacoustic (PA) technique which attracts great interest because it makes them suitable for many technological applications.

2. Experimental work.

2.1Materials

The materials used in the synthesis of Fe_3O_4 NPs are; ferric chloride hexahydrate ($FeCl_3 \cdot 6H_2O$), ferrous chloride tetra-hydrate ($FeCl_2 \cdot 4H_2O$),). Ammonium solution NH_4oH (26% of ammonia) from Analar (England). acetone from Molar Hungary), and nitrogen gas (N_2) with 99.9% purity. Deionized water was used for all experiments from India.

2.2. Synthesis of Fe_3O_4NPs

Co-precipitation is the most widely and simplest method for synthesis magnetics nanoparticles of controlled sizes by precipitate ferrous and ferric salts. Fe_3O_4 were prepared under nitrogen (N_2) gases bubbling through the solution to protect Fe_3o_4 against critical oxidation. 20.25 g ($FeCl_3 \cdot 6H_2O$), and 10.35 g of ($FeCl_2 \cdot 4H_2O$) were dissolved into 250 mL of distilled water. The solution stirring for 80 minutes, chemical precipitation was achieved at 90C under stirring by adding ammonium solution drop by drop at a constant rate until pH ranging between 8 and 14 Completed precipitation of Fe_3O_4 expected [19]. The system was cooled to room temperature, the precipitates were separated by a magnet and washed with distilled water until pH neutral. Finally, Fe_3O_4 washed with acetone and dried in an oven at 70-80C for 1.5 h to prepare the nanoparticles of Fe_3O_4 in powder form, the size and shape depend on the pH value of the solution. We get three different sizes labeled a, b and c. at PH 8-10, 11-12, and 13-14 respectively.

3-*Characterizations*

The absorption bands of the prepared samples have been measured by the UV-670 Jasco double-beam spectrophotometer utilizes a unique, single monochromator design covering a wavelength range from 190 to 2700 nm. The crystal structure of Fe_3O_4 NPs was characterized by X-ray Diffraction (XRD) (Shim ADZU diffractometer type XRD 6000. X-ray diffraction (XRD) is a well-known technique for the characterization of bulk and thin film. Transmission Electron Microscope (TEM) is used for characterizing the size of nanoparticles. TEM (JEOL JEM-2100 operated at 200KV with high-resolution Gatan CCD bottom camera, Orius SC200).

A highly sensitive (PA) technique has been utilized to investigate the thermal parameters (thermal diffusivity (α), thermal effusivity (e), and thermal conductivity (k) of Fe_3o_4 NPs of different sizes. The (PA) technique depends on the detection of pressure fluctuations in a sealed closed-cell created by the periodic thermal waves from the sample. The experimental set-up of the PA technique is shown schematically in figure (1).

The light beam from Stability 2017 Argon Laser was mechanically modulated by an optical chopper (SR540) and focused onto the sample which was mounted carefully inside a PA cell (MTEC Model 300). The sound wave generated from the sample were subsequently detected as an acoustic signal by a highly sensitive electrical microphone fixed in the PA cell. The PA signal was then amplified by a low noise preamplifier and further processed using a lock-in amplifier (Stanford Research System, Model SR830 DSP [20-21**].** The PA signal was recorded for varied frequency for each sample.

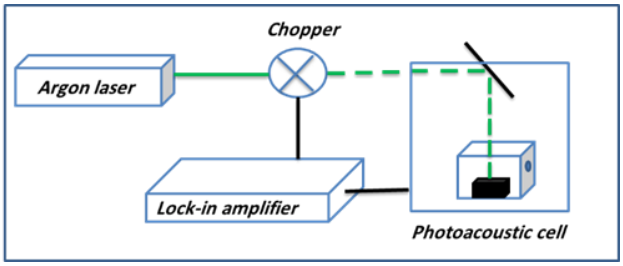

Figure 1. Photoacoustic Technique

4. Results and Discussion.

4.1 *TEM analysis*

TEM analysis has been used to determine the average particle size of Fe_3o_4 NPs The TEM micrographs of samples a,b and c are shown in Fig. 2a, 2b, and 2c respectively. The prepared nanoparticles' images show a nearly spherical morphology. The estimated particle size of a, b, and c samples are 10 nm, 20 nm, and 30 nm respectively.

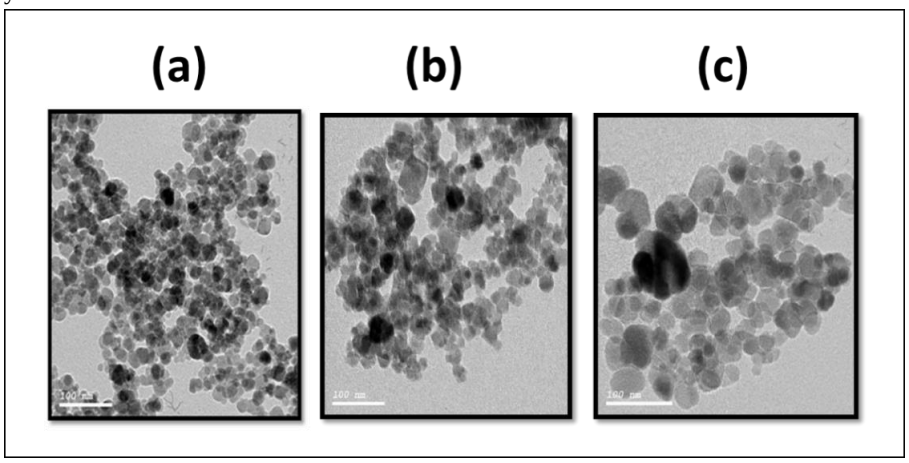

Figure 2. TEM images of the synthesized Fe_3O_4 NPs (a), (b), and(c)

4.2. *UV–Vis absorption*

Optical absorption spectra of samples show a broad absorbance (no sharp absorbance peaks) for all different sizes fig (3), which is mainly due to the half-metallic behavior of Fe_3O_4NPs [22]. The visible absorption is mainly because of the mixture of the ligand near-infrared absorption is assigned to the inter valence field transition and charge-transfer transition, while the charge-transfer transition between the metal ions. The absorption edges are 372 nm,383 nm, and 404 nm for the samples a, b, and c respectively

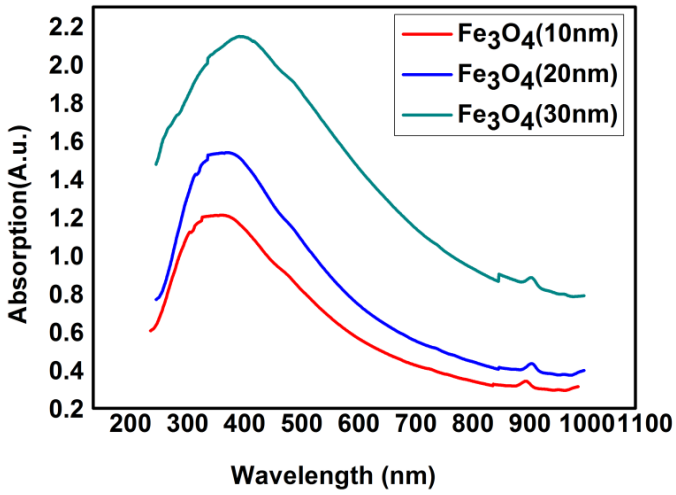

Figure 3. the absorption spectra of the prepared Fe3o4with different sizes 10,20and30nm respectively

The electronic transitions are the essential parameter of the optical absorption. These transitions are controlled by certain selection rules, which can be expressed by using Tauc's equation [23].

$$\alpha h\upsilon = A(h\upsilon - E_g)^n \qquad (1)$$

where $h\upsilon$ is the energy of the incident photons, α is the absorption coefficient, A is a constant, h is Planck's constant, and n is a constant with allowed values of 1/2 and 2 and not allowed values of 3/2 and 3 for direct and indirect transitions correspondingly. The values of n were detected in the range (0.925-1.083) which predicts the electronic allowed direct transition. The values of band-gap are determined by the Tauch-plot curve of $\alpha h\upsilon^2$ value on $h\upsilon$. The interception of the extrapolation of this linear part to the energy axis gives energy bandgap E_g Figure 4 shows the difference of $(\alpha h\upsilon)^2$ with photon energy $h\upsilon$ for the three samples (a,b, and c). The values of E_g for Fe_3o_4 NPs are 1.84, 1,73, and 1,47ev.

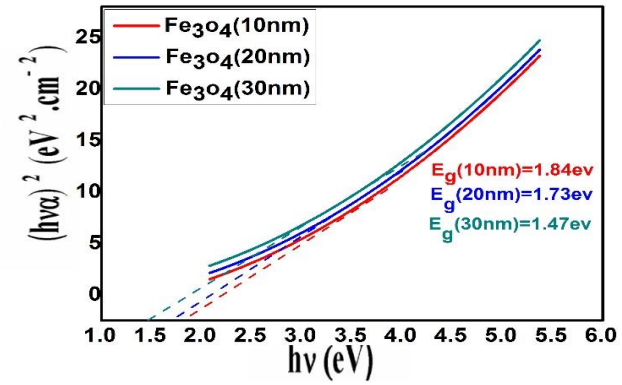

Figure 4. $\alpha h\upsilon^2$ was plotted versus hν for synthesized samples Fe_3O_4 NPs10, 20 and 30nm respectively

Using the calculated bandgap and the "Effective Mass Approximation" model (*EMA*) the size of Fe_3O_4 NPS is calculated**.** The EMA model is given by [24]**.**

$$E_{gn} = E_{gb} + \frac{h^2}{8R^2}\left[\frac{1}{m_e} + \frac{1}{m_h}\right] - \frac{1.8e^2}{4\pi\varepsilon\varepsilon_0 R} \qquad (2)$$

where Egn is the electronic bandgap for bulk Fe_3o_4 (0.1 ev), R is the average radius of NPs, m_e is the electron effective mass ($100m_o$), m_h is the hole effective mass ($100m_o$), $m_0 = 9.11*10^{-31}$ Kg and ε is the dielectric constant forFe_3O_4[24]. The calculated particles sizes are 10.3 nm, 20 .2 nm, and 30.3 nm which are comparable to those obtained by TEM measurements.

4.3 X-Ray diffraction analysis.

XRD measurements were used to recognize the crystalline structure of the products. Fig (5) showed that the XRD peaks can match fine with the characteristic peaks of the inverse cubic spinel (reflection peak at 2θ=35.6°) structure (JCPDS 19-629), which shows the crystalline structure of Fe_3O_4 NPs.

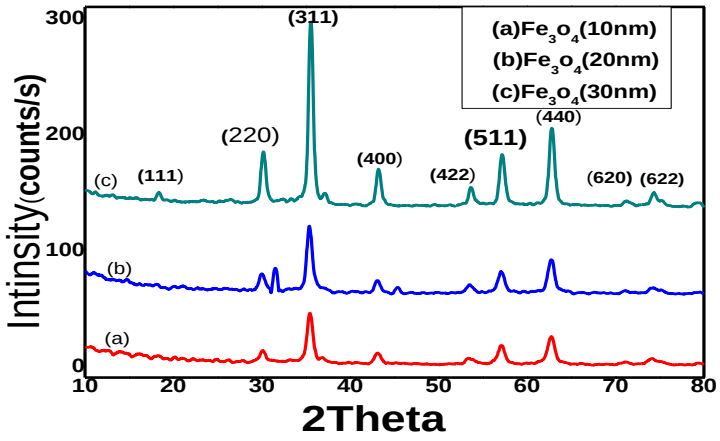

Figure 5. the XRD spectra of synthesized Fe_3o_4 with different sizes(a), (b)and(c) respectively.

pattern could be readily identified as the pure cubic phase of Fe_3O_4. The average crystalline size calculated using the Debye–Scherrer equation [25].

$$D = \frac{0 \cdot 9\lambda}{B\ cos\theta} \qquad (3)$$

Where β is the full-width at half-maximum (FWHM) value of XRD diffraction lines, the wavelength λ= 0.15405 nm and θ is the half diffraction angle of 2θ [26-28]**.** The value 2θ is the average of 30.1°,35. °6,43.2°,53.5°, and 56.95 at the diffraction peaks for each sample. The average crystalline size of Fe_3O_4 NPs is 10.7 nm, 20.20 nm, and 30.43nm in close agreement with TEM and optical measurements.

4.4 Thermal measurements

The thermal properties of Fe_3O_4 nanoparticles were studied with the Photoacoustic (PA) technique. The samples in powder form were compressed into disks (under a hydraulic pressure 30 Ton/inch) with the thickness (0.62 mm). For each appropriate (depth profile analysis) the PA signal amplitude was reported at different chopping frequencies (f). Fig 6 shows the plots of ln PA signal amplitude versus lnf for synthesized samples (a), (b), and (c) respectively. A distinct slope transition is observed at a frequency f_c (the sample transitions from thermally thick to thermally thin) where the crossover occurs. The thermal diffusivity (α), for all samples, was then calculated using the relation [29].

$$\alpha = f_c L^2 \qquad m^2/sec \qquad (4)$$

where *L* is the thickness of the sample. The measured values of α are shown in Table 1. It easily observes that as the size of Fe_3o_4 NPs increase the thermal diffusivity increase.

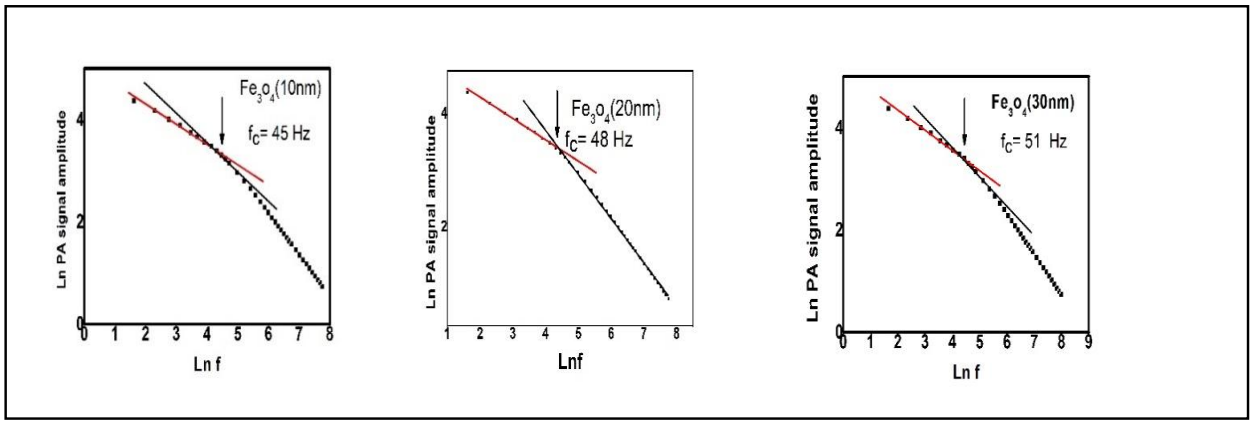

Figure 6. ln PA signal amplitude versus lnf for synthesized Fe_3O_4 10,20&30nm respectively

The thermal effusivity (e) of the samples was also calculated using the PA technique, where the PA signal amplitude q is given for optically opaque and thermally thick samples by [30- 32]

$$q = \frac{B}{e}\frac{1}{f} \qquad (5)$$

where $B = \frac{I_0}{2}\frac{\gamma P_0 \alpha_g^{1/2}}{2\pi l_g T_0}$,(I_0) is the incident light strength, (ϒ) is the specific heat ratio, (P_0) is the ambient pressure, (α_g) is the gas thermal diffusivity, (l_g) is the length of the gas column, (T_0) is the ambient temperature and (f) is the modulation frequency. Using Si as a reference sample, with 15670 $Ws^{1/2}m^{-2}K^{-1}$ thermal effusivity [29]. The Si reference sample is used to extract the B constant.

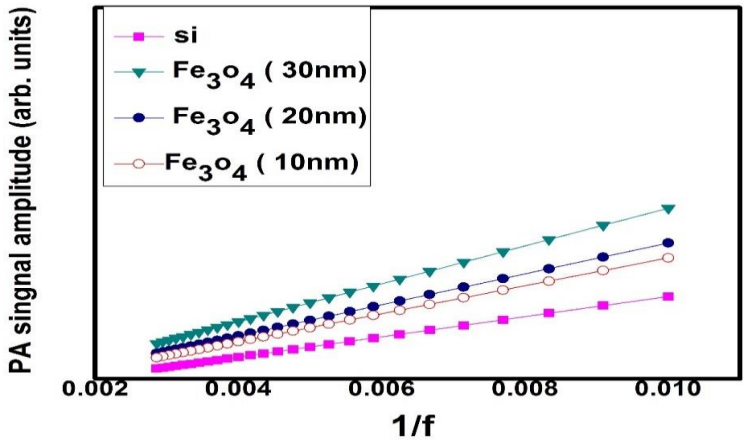

Figure 7. the variation of PA signal amplitude with inverse frequency for the reference sample and prepared NPs.

Fig (7) show the relationship between the PA signal amplitude and the inverse of the chopping frequency for reference sample (si) and three different sizes of Fe_3o_4, the slopes were obtained by linear fitting for the relation between (1/chopping frequency) and PA amplitude. The resultant thermal effusivities are given in table 1. The equivalent values of thermal conductivity $K=e\sqrt{\alpha}$ are calculated and given in table (1)

Table1. The measured values of the three Parameters for different sizes of Fe_3o_4 NPs

Sample Fe_3o_4	Thermal diffusivity (α) (10^{-5} m^2/s)	Thermal effusivity (e) (10^3 $Ws^{1/2}$ m^{-2} K^{-1})	Thermal conductivity (k) (W/m.K)
10nm	1.72	1.18	4.9
20nm	1.84	1.28	5.5
30nm	1.96	1.35	6

The values of (α.e and k) are increasing as the size of nanoparticles increases and decreases from its bulk value. The value of (k) for sample c is about 66 % from bulk value (9.7W/mK) [33]. Such decreases in (k) of Fe_3O_4 NPs from the bulk value are agreement with N. Rajkumar et al [33]. In their work, they obtained a decrease in (k) about 59 % for particles size 10 nm from the bulk value. In such a study, they explained the decrease of k of Fe_3O_4 NPs from the bulk value based on phonon. When the particles are small, phonon confinement increases, and thus the collision rate increases (mean free path decreases) resulting in reduced thermal conductivity. Moreover, As the size of the nanomaterial decrease, the surface-to-volume ratio increases, and the presence of increased surfaces due to roughness additionally provides the phonon with a scattering mechanism. This additional scattering decreases the mean free path of the phonon which causes the resistance in the heat flow resulting in a reduction of the thermal diffusivity and conductivity [34 - 35].

Conclusion

Magnetite nanoparticles synthesized by chemical co-precipitation method. The prepared Fe_3O_4(NPs) nanoparticles were characterized by TEM, UV-vis, and XRD. The average particle sizes estimated by TEM images are 10 nm,20 nm, and 30 nm. The UV-vis absorption spectra of Fe_3O_4 shifted toward the visible region and the redshift of broad an absorbance spectrum to longer wavelength with increasing particle size. The particle sizes are confirmed by an effective mass approximation model and XRD data. Furthermore, the Photoacoustic (PA) technique has been used to study the thermal diffusivity (α), thermal effusivity (e), and thermal conductivity (k) of Fe_3O_4 NPs. The values of (α.e and k) are increasing as the size of nanoparticles increases and decreases from its bulk value. The value of (k) for sample c is about 66 % of the bulk value it decreases with a decrease in particle size. The decrease in thermal conductivity as the particle size decreased is due to the increase in phonon containment and thus the increase in collision rate (mean decrease in the free path) leading to a decrease in thermal conductivity.

References

[1] Kim, J, K., Lee, J, H., & Lee, S, H. (2004). Journal of Magnetism and Magnetic Materials, 279(2-3), 173-177.

[2] Zargar, M., Hamid A, A., Bakar F, A., Shamsudin, M, N., Shameli, K., Jahanshiri, F., & Farahani, F. (2011). Molecules journal,16(8),6667–6676.

[3] Makovec, D., Kosak, A., &Drofenik, M. (2004). International Journal of Nanotechnology,15, S160-S166.

[4] McMichael, R, D., Shull, R, D., Swartzendruber, L, J., Bennett, L, H., &Watson, R, E. (1992). Journal of Magnetism and Magnetic Materials,111(1-2), 29-33.

[5] Shen, L., Laibinis, P, E., &Hatton, T, A. (1999). Langmuir,15, 447.

[6] Chou, S, Y., Wei, M, S., Krauss, P, R., & Fischer, P, B. (1994). Journal of Applied Physics, 76(3), 6673-6675.

[7] Raj, K., & Moskowitz, R. (1990). Journal of Magnetism and Magnetic Materials, 85(1-3), 233-245.

[8] Wang, X., Peng, Q., & Li, Y. (2005). Crystal Growth and Design Journal, **5**(2), 391-393.

[9] Ferreira, H, A., Graham, D, L., Freitas, P, P., & Cabral, J, M, S. (2003). Journal of Applied Physics,93(10), 7281-7286.

[10] Zhang, L., Dong, W, F., &Sun, H, B. (2013). Nanoscale journal,5(17),7664–7684.

[11] Jain, T, K., Morales, M, A., Sahoo, S, K., Leslie- Pelecky, D, L., & Labha-salwar, V. (2005). Molecular Pharmaceutics,2(3), 194-205.

[12] Kim, D, K., Mikhaylova, M., Wang, F, H., Kehr, J., Bjelke, B., Zhang, Y., Tsakalakos, T., & Muhammed, M. (2003). Chemistry of materials. Mater, 15(23), 4343-4351.

[13] Masala, O., & Seshadri, R. (2005). Chemical physics letters, 402(1-3), 160-164.

[14] Gope, P, C., Singh, V, K., & Rao, D, K. (2015). Journal of Reinforced Plastics and Composites,34(13): 1075-1089.

[15] Badawi, A., Al-Hosiny, N., Abdallah, S., Negm, S., & Talaat, H. (2012). Journal of Materials Science and Engineering, 2 (1) 1-6.

[16] Mandelis, A., Teng, Y, c., & Royce, b, S. (1979). Journal of Applied Physics, 50 (11), 7138-7146.

[17] Rosencwaig, A., & gersho. (1876). Journal of Applied Physics, 47,64.

[18] Sathyamoorthy, R., Sudhaga, r P., Saravana, R., & Sathy, T, M. (2010), Journal of Advanced Research, 46, 99 – 103.

[19] Sophie, L., Delphine, F., Marc, P., Alain, R., Caroline, R., Luce, V, E., N. & Robert, M. (2008). Chemical Reviews, 108, 2064-2110.

[20] okasha, A, M., T, Abdallah., Mohamed, M, B., Anis, B, B., Negm, S., & Talaat, H.(2010).journal of physics. conference series,214,19-23.

[21] Abdallah ,S., Abdallah, T., Mohamed ,M ,B., & Negm ,S .(2008). The European physical journal , 8,365-368.

[22] Hsia, C, H., Chen, T, Y., & Song, H. (2008). Nano Letters journal,8(2), 571-576.

[23] Ahmadi, M., Ghasemi, M, R., & Rafsanjani, H, H. (2011). Journal of Materials Science and Engineering,5,87-93.

[24] Lahore, P., & Jain, p. (2015). International journal Research Chemistry and Environment,4,38-43.

[25] El Ghandoor, H., Zidan, H, M., Mostafa, M, H., & Ismail, M, I. (2012). International Journal of Electrochemical Science, 7, 5734 – 5745.

[26] Victoria, L., Calero, C., & Carlos, R. (2007). Journal of Magnetism and Magnetic Materials,314, 60.

[27] Zhang, Y., Yang, Z., Liu, Y., ChunLong, F., &Yan, G. (2010). Journal of Magnetism and Magnetic Materials,322(22), 3470-3475.

[28] Kumar, V., Rana, A., Yadav, M, S., &Panta, R, P. (2008). Journal of Magnetism and Magnetic Materials, 320(11), 1729-1734.

[29] Almond, D, P., & Patel, P,.M (1996). champman& Hall series in accounting,13,978-8808

[30] Abdallah, S., (2004). Egyptian journal of solids,27,451.

[31] Awad, H., Abdallah, T., Mohamed, M, B., Easawi, K., Negm, S., & Talaat, H.(2010).journal of physics: conference series,214(1),012130.

[32] Abdallah, S., easwi, k., Negm, S., Youssef, G, M., El-brolossy, T, A., & H, talaat. (2003). Review of scientific insturments,74,848.

[33] Rajkumar, N., Umamahaeswari, D., & Ramachandran, K. (2010). International Journal of Nanoscience, 3,243–250.

[34] Arora, N.**,** Deepika, P, J., & Pachauri, U. (2018). Materials Chemistry and Physics,217,235-241.

[35] Arabshahi, H. (2011). International Journal of the Physical Sciences, 6(13), 3155–3161